Archives of Acoustics Vol. 51, No. 1, pp. 3–23 (2026), https://doi.org/10.24423/archacoust.2026.4190

Research Paper

Application of Acoustic Metamaterials in the Design of Muffling Unit of Internal Combustion Engine

Tianshuo Li, Lei Zheng*, Zhengyang Bi, Hongchao Ji

College of Mechanical Engineering, North China University of Science and Technology
Tangshan, Hebei, China

*Corresponding Author: zhenglei1@163.com

Received February 13, 2025; revised October 29, 2025; accepted November 24, 2025; available online January 15, 2026; version of record March 17, 2026; published issue March 27, 2026.

Aiming at the problems of large volume, high exhaust resistance and difficulty in suppressing noise in the 500 Hz to 100 Hz frequency band of traditional internal combustion engine exhaust mufflers, a noise reduction unit design based on acoustic metamaterials is proposed. Based on the equivalent medium theory, an acoustic model with a ring structure and multi-region variable refractive index was established. Phase control is achieved by helically winding the acoustic channel to change the refractive index, and the basic dimensions of the acoustic metamaterial muffling unit are calculated. The sound field distribution, transmission loss and flow field characteristics of the muffling unit are simulated and analyzed. This structure utilizes a multi-layer acoustic channel structure, effectively alleviating the problem of insufficient low-frequency noise elimination caused by the asymmetry of Fano interference. It achieved a transmission loss of over 10 dB within 85 % of the 500 Hz to 1000 Hz frequency band, and still maintained excellent noise reduction performance under high-frequency conditions through multi-level phase control. By connecting multiple units in series, a transmission loss of 10 dB can be achieved within 85 % of the 500 Hz to 1000 Hz frequency band. The exhaust flow field of the muffling unit was simulated and analyzed. Whether used alone or in series with the traditional muffling structure, the exhaust resistance remained within the range of 360 Pa to 370 Pa. Experimental tests show that when the metamaterial muffler unit is used in combination with the traditional muffler, it effectively achieves targeted noise elimination in the 500 Hz to 1000 Hz frequency band, and also demonstrates clear noise reduction capabilities in higher frequency ranges. The high noise suppression characteristics, high gas passage characteristics and compact volume characteristics of this structure provide more potential analysis methods and design schemes for the research and development of internal combustion engine mufflers and noise reduction accessories.

Keywords: acoustic metamaterials, muffler, transmission loss, exhausting resistance.

1. Introduction

Internal combustion engine noise has always been one of the significant sources of urban noise pollution (Wan *et al.*, 2023), among which exhaust noise has always accounted for a considerable proportion in engine noise emissions (Narayan *et al.*, 2021). Mufflers can suppress noise while ensuring exhaust capacity. However, the structural design of the noise reduction units is restricted by multiple performance indicators, such as noise reduction frequency, structural dimensions, acoustic performance, and aerodynamic performance (Zhang *et al.*, 2018).

The traditional structure design of mufflers is generally based on the acoustic wave equation, using reflection and interference methods to achieve the cancellation of sound waves (Araujo, Pestana, 2024; Li *et al.*, 2024; Lee *et al.*, 2020); through the Helmholtz resonance principle to absorb the vibration energy of sound waves

(Bai *et al.*, 2023; Kheybari, Ebrahimi-Nejad, 2019) or based on the small hole injection theory to shift the vibration sound waves to high frequencies and ultra-high frequencies (Chen *et al.*, 2020; Wang *et al.*, 2012). Under high-speed exhaust conditions, these structures will increase the exhaust resistance of the engine. Meanwhile, due to the longer wavelength of low-frequency noise and the fact that high-temperature exhaust conditions make this issue more prominent, this imposes certain limitations on the spatial structure and size design of the muffler when eliminating noise with frequencies below 1000 Hz. However, human hearing has different loudness responses to noise of different frequencies. Noise ranging from 500 Hz to 2000 Hz has a higher loudness. Therefore, noise elimination under the frequency conditions of 500 Hz to 1000 Hz has become a difficult point in the muffler of internal combustion engines. However, these muffler structures will inevitably cause an increase in the exhaust resistance of the energy engine. Martos *et al.* (2023) showed in his study on the exhaust back pressure of Euro 6 diesel engine that when the back pressure was increased from about 4500 Pa to 12 500 Pa, the average effective pressure (BMEP) of the engine under the medium load condition of 2000 rpm decreased by about 10 %. Dalla Nora *et al.* (2016) showed in the study of backpressure sensitive two-stroke GDI engine that the exhaust resistance of the engine has a significant impact on the performance of the engine under the condition of 800 rpm and 2000 rpm. Under the condition of 800 rpm, when the backpressure is increased from 104 Kpa to 120 Kpa. The power and efficiency of the engine have both decreased by 15 % to 20 %.

Especially when multiple muffler structures are connected in series, the contradiction between the acoustic effect of the muffler, its spatial volume and exhaust resistance becomes more prominent (Liao *et al.*, 2024; Su *et al.*, 2020).

Acoustic metamaterials, also known as acoustic artificial structure or Acoustic Metamaterials, applied the principle of optical metamaterials and based on the theory of equivalent media, acoustically artificial designed structural units arranged individually or with periodic array are adopted (Liu *et al.*, 2020), as shown in Fig. 1. Through complex spatial structures or combinations of multiple media, the equivalent acoustic parameters, such as the equivalent volume modulus and the equivalent elastic modulus, are changed to change the sound field (Fang *et al.*, 2006; Ye *et al.*, 2020; Orazbayev, Fleury, 2020; Zeng *et al.*, 2013).

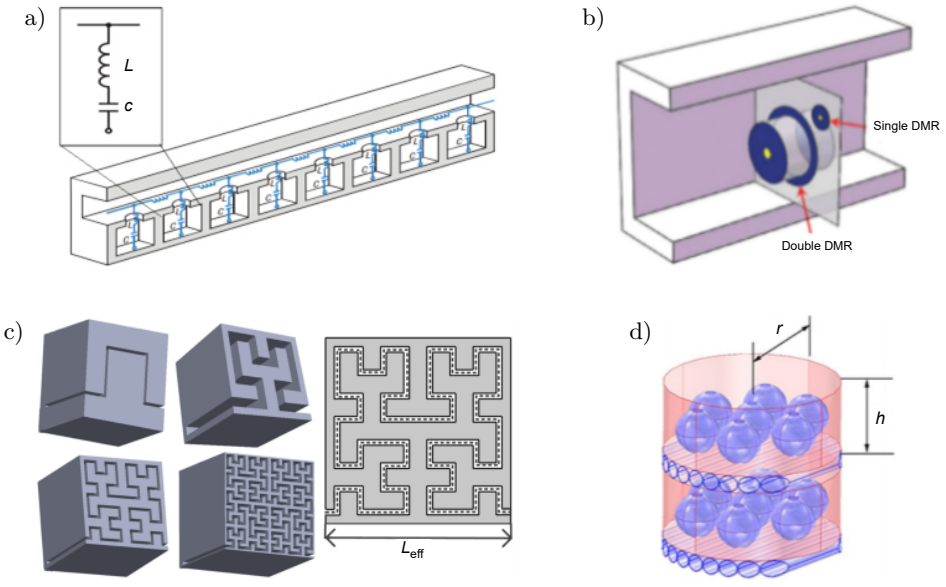

Fig. 1. Various types of acoustic metamaterials: a) local resonance, b) thin film, c) spatially coiled, d) supramolecular.

Acoustic metamaterials can achieve better acoustic effects in the fields of sound field control, sound absorption and sound insulation, especially in the aspects of abnormal reflection refraction of sound waves, compact sound absorption structure, etc. At the same time, it also provides certain ideas in ventilation and sound insulation, especially in the aspect of noise reduction with large porosity, such as: local resonance model (Jiang *et al.*, 2023; Li *et al.*, 2022; Liu *et al.*, 2019; Zhang *et al.*, 2024) and phase regulation model (Guo *et al.*, 2023; Xu *et al.*, 2021).

Mohamad *et al.* (2021) combined acoustics and fluid mechanics to analyze the system back pressure increase behavior caused by Helmholtz resonance near the small hole during the muffling process of the perforated pipe. Under the exhaust gas velocity condition of 40 m/s, the perforated pipe model would lead to a pressure loss of 795 Pa to 889 Pa. Meanwhile, the research shows that the secondary noise caused by the increased resistance will lead to a 10 % increase in the outlet sound pressure level. Sun *et al.* (2020) pointed out that interference based on local resonance only works at resonant frequencies, which means that there is only a narrow operating frequency range near each noise suppression interference frequency. Considering that noise is usually broadband noise, there are still certain challenges in designing acoustic ventilation structures for broadband. The muffler based on the phase control principle has greater advantages in gas permeability.

Zhang *et al.* (2024) proposed a combined acoustic metamaterial (CAM) based on multi-channel Fano resonance. By coupling helical channels with hollow structures, it achieves broadband sound insulation of >13 dB in the 520 Hz to 989 Hz frequency band while maintaining a ventilation rate of 63 %. Experimental verification shows that its peak acoustic transmission loss reaches 62 dB, providing a lightweight solution for traffic noise control.

Ghaffarivardavagh *et al.* (2019) proposed a super-open acoustic metamaterial (UOM) based on the Fano interference effect. By comparing the acoustic impedance of the central ventilation hole (60 % open area) with that of the spiral channel. It achieves a 94 % acoustic energy attenuation at 460 Hz (with a STL peak of 26 dB), providing a highly breathable solution for ventilation and noise reduction structures.

Although the operating frequency range is expanded by inducing multiple resonances, the airflow channel is weakened to a large extent, and the phase-controlled structure can provide greater porosity while supporting broadband noise cancellation. For spiral metamaterials, the plane space of traditional acoustic metamaterials is folded and extended to the 3D space, which greatly improves the space utilization rate. The higher center hole area is obtained, so it is more suitable for the basic structural unit of internal combustion engine exhaust noise reduction. Xu *et al.* (2025) combined the Archimedes spiral with the ventilation function and verified through experiments the balance between broadband noise reduction and high ventilation efficiency of the spiral metamaterials, providing a new geometric configuration reference for the design of ventilation and noise reduction units. Lu *et al.* (2025) combined Fano resonance with 3D expansion, solving the problems of the single shape and difficulty in practical application of traditional Fano-type mufflers, providing a theoretical basis for the modular design and 3D layout of ventilation mufflers. The above research indicates that the acoustic suppression device based on the principle of phase interference essentially does not eliminate sound but blocks its passage, enabling energy consumption at any point before the blocking point. Its high flowability is suitable for engine exhaust passages with high-speed and low-resistance requirements.

It can be seen from this that the medium and low-frequency components in the exhaust noise of internal combustion engines, due to their longer sound wave wavelengths, the traditional noise reduction technology based on pipe length tuning is difficult to meet the compact design requirements of modern power systems. However, acoustic metamaterials have a more compact structure and more efficient noise reduction capabilities, and the phase control model within them can provide a higher gas high pass rate. Therefore, based on the equivalent medium theory of acoustic metamaterials, we take advantage of the phase control structure and, under the premise of maximizing the utilization of space, design a low-resistance muffler with a hollow structure to achieve targeted noise elimination in the 500 Hz to 1000 Hz frequency band of internal combustion engines. This not only compensates for the current noise defect of internal combustion engine scheduling, but also provides an effective idea for wideband noise reduction of pipelines.

2. Structure design of noise reduction unit based on equivalent medium theory

2.1. Basic principles of acoustic metamaterials

The phenomena such as reflection and transmission in homogeneous media can be solved by mathematical equations in the classical propagation theory, but the propagation characteristics are difficult to analyze

when the medium is non-homogeneous. At this time, the inhomogeneous medium is treated as a homogeneous medium under some approximate conditions, which provides a solution to the problem. In this way, the equivalent medium theory is developed, which is also an important theoretical basis for the study of metamaterials. Therefore, the metamaterials of this array arrangement are equivalent to a uniform medium, which is also called metamaterials.

The concept of metamaterials was initially introduced into the field of optics to deal with electromagnetic waves using materials with negative dielectric constants and negative magnetic permeability. For a monochromatic wave in an isotropic medium, the square sum dispersion relation of the refractive index is (Li *et al.*, 2014):

$$k_s^2 = \frac{n_s^2 \omega^2}{c^2}, \tag{1}$$

where k_s is the wave number, n_s is the refractive index, ω is the frequency, c is the speed of light.

Since both electromagnetic wave and acoustic wave satisfy the wave equation, they have a large number of analog characteristics. This theoretical knowledge can be applied to acoustic wave, and acoustic metamaterial characteristics can be theoretically obtained, and the formula of acoustic refractive index can be obtained as follows (Chen *et al.*, 2024):

$$n_s^2 = \frac{\varepsilon}{\mu}, \tag{2}$$

where $\varepsilon$is the dielectric constant (in optics) and also the mass density (in acoustics), μ is the magnetic permeability (in optics) and also volume elastic modulus (in acoustics).

As shown in Fig. 2, in the first quadrant, the wave propagates normally in the pipeline with positive mass density and bulk elastic modulus ($\rho > 0$, $K > 0$). In the second quadrant, when the Helmholtz resonator structure is adopted, the resonant sound wave generated through the resonator is opposite to the incident sound wave, and the local force of the sound wave is opposite to its vibration acceleration direction ($\rho < 0$, $K > 0$), the refractive index is imaginary, and the sound wave propagation is terminated, that is, the sound attenuation is realized. In the fourth quadrant, when the thin film structure is used, when the vibration frequency of the thin film is opposite to the vibration frequency of the sound wave, the volume of the thin film will expand under pressure and shrink under tension ($\rho > 0$, $K < 0$), resulting in the sound wave stopping propagation (Naify *et al.*, 2012). In the third quadrant, the two structures exist at the same time, which presents a double negative characteristic ($\rho > 0$, $K < 0$). At a specific frequency, the sound wave can continue to propagate, but the acoustic refractive index will change, so as to achieve special functions such as acoustic lens (Wang *et al.*, 2024).

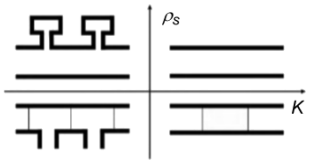

Fig. 2. Quadrant diagram of equivalent acoustic parameters.

From Eq. (1) and Eq. (2), it can be seen that when the dielectric constant or magnetic permeability is negative, the square of the refractive index remains negative, that is, the refractive index is an imaginary number, and the wave propagation stops. When both the dielectric constant and magnetic permeability are negative, the square of the refractive index remains positive, that is, the refractive index is still a real number. The propagation of the wave can continue, but the propagation characteristics will change. It is precisely this feature that provides the theoretical condition for phase control to achieve the muffler of the internal combustion engine displacement (Shaikh *et al.*, 2024).

The concept of acoustic metamaterials is not limited to locally resonant materials or periodic structures. Sound waves in a fluid are longitudinal scalar waves, and unlike electromagnetic waves, acoustic waveguides have no cut-off frequency and can limit their path through narrow channels at will. By limiting the sound path and adjusting the phase of the sound wave, the transmission track with negative dispersion characteristics ($\rho < 0$, $K < 0$)

can be folded and compressed into the subwavelength range (Kumar, Lee, 2020), such as the spatial winding metamaterials, topological acoustic metamaterials, fractal acoustic metamaterials, spiral metamaterials and acoustic metasurface. For the helical spatial acoustic metamaterials, the incident sound wave is confined to the helical subwavelength cross section channel wound in 3D space, resulting in the phase delay of the sound wave propagating along the slender path, thus achieving a higher acoustic refractive index. The phase delay is calculated as

$$\Delta\varphi = 2\pi k l_0, \tag{3}$$

where $\Delta\varphi$ is phase delay and l_0 is the valid channel length.

2.2. Design of equivalent medium theoretical model for acoustic metamaterials

In order to regulate the phase of sound waves in different acoustic transmission areas, the sound attenuation is realized through the strongly coupled dipole vibration. The acoustic model of the acoustic attenuation unit can be equivalent to the theoretical model of the radial double-layer material structure, as shown in Fig. 3. According to the effective medium theory, the central part and the surrounding part are characterized by refractive indices n_1 and n_2, respectively.

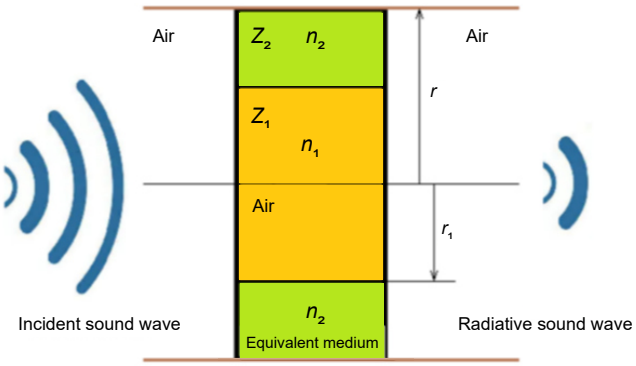

Fig. 3. Equivalent medium model of muffler element.

Since the acoustic metamaterial unit is a subwavelength scale, the vibration of the acoustic metamaterial unit can be characterized by the characteristic mode function and the characteristic frequency by its Green function (Yang *et al.*, 2013):

$$G(h,h') = \sum_n \frac{p_n(h)p_n^*(h')}{(\omega_n^2 - \omega^2)/B_n}, \tag{4}$$

where $p_n(h)$ and $p_n^*(h')$ are the n-order eigenmodular functions and their conjugations at positions h and h', ω_n is the characteristic frequency of the n-order, B_n is the average modulus of the n-order eigenmodulus:

$$\frac{1}{B_n} = \frac{\int p_n(h)\, p_n^*(h)\, \mathrm{d}v}{B_0 s}, \tag{5}$$

where s is the cross-sectional area of the unit, B_0 is the volume modulus of air, $B_0 = \rho_0 c_0$, ρ_0 is the air density, and c_0 is the air sound velocity.

Vibration in acoustic metamaterial units can be expressed through monopole and dipole modes (Yang *et al.*, 2014):

$$\overline{G}_+ = \omega^2 \sum_n \frac{p_n^*(h)\,[p_n(h) + p_n(-h)]}{(\omega_n^2 - \omega^2)/B_n}, \tag{6}$$

$$\overline{G}_- = \omega^2 \sum_n \frac{p_n^*(h)\,[p_n(h) - p_n(-h)]}{(\omega_n^2 - \omega^2)/B_n}, \tag{7}$$

where h is the axial position coordinate of the acoustic metamaterial unit.

Based on the effective medium theory, the acoustic metamaterials unit can be equivalent to a homogenized medium of the same thickness, where the effective wave number $\overline{k}$ satisfies the equation:

$$\left(\frac{\partial^2}{\partial x^2} + \overline{k}_s^2\right)\overline{p}\,(z) = 0. \tag{8}$$

Then the wave number can be determined by the unipolar mode and dipolar mode as (Sun *et al.*, 2020):

$$\overline{k}_s = \frac{1}{h}\operatorname{arccot}\sqrt{-\frac{\overline{G}_+}{\overline{G}_-}}. \tag{9}$$

Effective impedance $\overline{Z}$ can be expressed as

$$\overline{Z} = -\frac{\overline{G}_+}{\omega\cot\left(\overline{k}_s h\right)}. \tag{10}$$

Finally, the transmission coefficient of the acoustic metamaterials unit is obtained (Xiao *et al.*, 2013):

$$T = \frac{4e^{2ih\overline{k}_s}\overline{Z}Z_0}{\left(\overline{Z}+Z_0\right)^2 - e^{4ih\overline{k}_s}\left(\overline{Z}-Z_0\right)^2}, \tag{11}$$

where Z_0 is the acoustic impedance in the air, $i = \sqrt{-1}$.

Correspondingly, the transmission loss equation is

$$\mathrm{TL} = 10\log_{10}\left(\frac{W_i}{W_t}\right) = -20\log_{10}|T|, \tag{12}$$

where W_i is the incident sound power, W_t is the transmitted sound power, T is the transmission coefficient.

From Eq. (11) and Eq. (12), it can be known that we have two methods to achieve noise reduction. The first approach is to increase the impedance of the air or metamaterial to create a significant difference, thereby reducing the transmission coefficient T and increasing the transmission loss TL. This is not easy to achieve under the condition of ventilation. The second approach is to set the real part of the transmission coefficient to zero and retain only the imaginary part. This processing method can also suppress the propagation of sound waves, which is exactly the effect we expect. To this end, we need to adjust the value of $h\overline{k}_s$ in $e^{2ih\overline{k}_s}$ so that there exists a relationship of $2hk = (2n+1)\pi$, which makes the imaginary part of the exponent of the factor $e^{2ih\overline{k}_s}$ equal to $(2n+1)\pi$.

When $\overline{G}_+ = \overline{G}_-$, the effective wave number becomes pure virtual infinite, then $\overline{k} \to \infty$, which indicates that the system has the same monopole and dipole response intensity, and the extreme attenuation of the incident wave is the complete block of the acoustic metamaterials unit. At this point, the impedance expressed by Eq. (10) is infinite, while the real part of the expressed transmission coefficient expressed by Eq. (11) is 0. The transmission loss expressed in Eq. (12) is the imaginary part of the transmission coefficient T, which is a relatively large value at this time. This provides a theoretical basis for sound field elimination for us to achieve noise reduction during the displacement of internal combustion engines.

2.3. Structural design of acoustic metamaterials muffling unit

If we want to achieve noise reduction in the 500 Hz to 1000 Hz frequency band of internal combustion engines through the model shown in Fig. 3, there are still two significant problems. Firstly, we need to find the corresponding material or structure of the equivalent medium in reality. Secondly, we also need to extend the noise reduction frequency of this model to the 500 Hz bandwidth.

2.3.1. Design of equivalent media

Although it is difficult to obtain high refractive index acoustic materials in the outer ring of the equivalent medium model in reality, the acoustic metamaterials wound in space can be utilized to extend the acoustic wave

transmission path, equivalently achieving a sound velocity significantly lower than that in the central region and a nearly zero acoustic refractive index. This enables the regulation of the incident acoustic wave phase and the realization of dipole vibration at the exit with a certain phase difference from the central channel. The spiral spatial winding structure can maximize the utilization of axial space and is more suitable for the structural requirements of exhaust noise reduction.

For the acoustic channel of the central cylindrical tubular structure and the acoustic channel of the outer ring spiral structure, there is an approximate proportional relationship between the acoustic impedance value (Ghaffarivardavagh *et al.*, 2019):

$$\frac{Z_2}{Z_1} = \frac{\pi_1^2}{l\,(r - r_1)}, \tag{13}$$

where Z_2 is the acoustic impedance of the outer loop spiral channel, Z_1 is the acoustic impedance of the central channel, and r_1 is the diameter of the central channel, r is the diameter of the outer ring, and l is the pitch of the spiral structure. When the ratio of Z_2/Z_1 is close to 1, the acoustic vibration response intensity of the two regions can be obtained respectively through impedance balance. To achieve noise reduction over a wider frequency range, we reduced the impedance of part Z_2 (Khodabakhsh *et al.*, 2025; Lin *et al.*, 2024) to make the value of Z_2/Z_1 is 0.6, which also provided the preparatory conditions for us to expand the design of the outer ring structure into multiple channels.

According to Eq. (3), the acoustic channel length is used to control the phase. According to the trigonometric relationship between the length and height of the helix structure, the acoustic refractive index n_s can be expressed as

$$n_s = \frac{1}{\cos\beta}, \tag{14}$$

where β is spiral angle.

To achieve noise elimination in the frequency range of 500 Hz to 1000 Hz and minimize the volume to the extreme, we have designed a helical structure muffler. When the exhaust pipe temperature is 350°, the sound velocity is approximately 550 m/s. Taking the conventional exhaust pipe inner diameter (internal diameter) of 5 cm as the design standard, the basic dimensions of the acoustic metamaterials muffling unit are obtained as follows: l = 11.2 cm, r_1 = 2.5 cm, r = 5.5 cm, and the spiral angle is 3.6π. The basic dimensions of the acoustic metamaterials muffling unit is shown in Fig. 4. However, the external center diameter of this structure is 8 cm, and the corresponding center noise reduction frequency is 843 Hz. The theoretical noise reduction frequency is between 550 Hz and 1050 Hz.

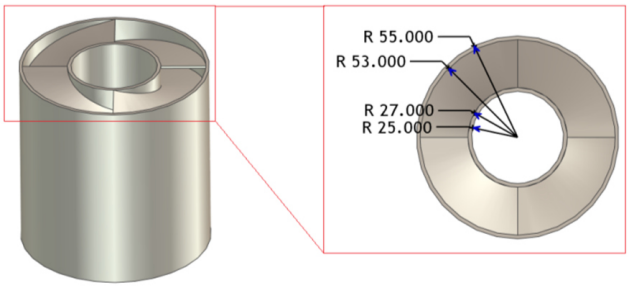

Fig. 4. Basic dimensions of the acoustic metamaterial muffling unit.

2.4. Design of wideband noise reduction

Although incomplete coupling can achieve a wider noise reduction frequency range, due to the asymmetry of Fano interference, the transmission loss in the low-frequency region decays too quickly, and thus an effective noise reduction effect cannot be obtained. To achieve noise reduction in lower frequency bands under the same volume conditions, further, we adopt a multi-channel structure to obtain multiple noise reduction frequency bands, weakening the influence of Fano interference asymmetry. As shown in Fig. 5, the outer ring area is radially divided into multiple acoustic channels to enhance the targeting of the noise reduction frequency.

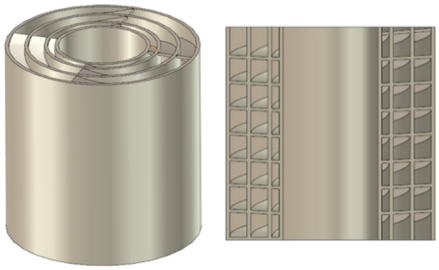

Fig. 5. Acoustic metamaterial muffling unit model.

According to the trigonometric relationship of the spiral development line, different acoustic channels correspond to different spiral outer diameters, respectively corresponding to different spiral angulation β:

$$\cos\beta = \frac{H}{2\pi r}, \tag{15}$$

where H is the spiral height, r is the spiral radius.

By bringing Eq. (15) into the relation between refractive index and spiral radius shown in Eq. (14), the relation between channel radius and acoustic refractive index can be obtained at a fixed height:

$$n_s = \frac{2\pi r}{H}. \tag{16}$$

For the multi-channel phase-controlled noise reduction structure, because each layer acoustic channel corresponds to different acoustic refractive index output and phase difference, multiple noise reduction frequency bands can be superimposed to make the noise reduction frequency band distribution more uniform.

Therefore, without changing the original overall structure, we segmented the outer ring channel and obtained the structures of two-layer and three-layer outer ring channels, respectively. The final size is shown in Fig. 6, which achieves phase shift of multiple channels to enhance the sound suppression ability of the 500 Hz and 1000 Hz frequency bands.

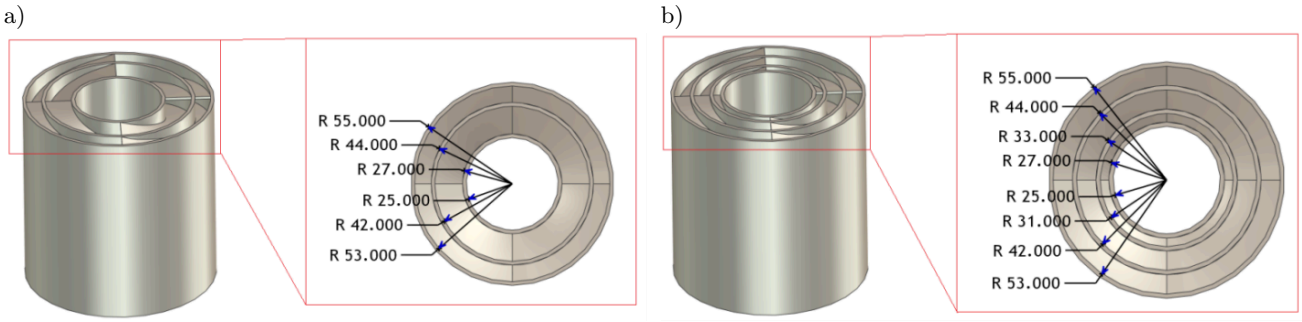

Fig. 6. Different outer ring channel structures: a) two-layer outer loop channel, b) three-layer outer loop channel.

3. Simulation analysis of acoustic performance of muffling unit

In order to more intuitively understand the coupling process and sound field distribution of sound waves generated by phase regulation of different acoustic channels at the exit, an acoustic metamaterial muffler model was established, and a simulation analysis of the sound pressure level and sound field was carried out by Harmonic Acoustics of ANSYS workbench 2020.

3.1. Simulation model, mesh, and parameter settings

The model medium is air, with the sound velocity set at 550 m/s. The acoustic input is set at the inlet end, and the radiation boundary is set at the outlet end. All walls are assumed to be rigid walls. The model is divided

into grids, with the grid type being tetrahedral grids and the grid size being 5 mm. The total number of grid elements is 164 000. The structure and grid of acoustic metamaterials muffling unit model is shown in Fig. 7. The model parameter is shown in Table 1. And monitor the sound field difference in the red wireframe area, as well as detect the sound pressure level difference between the outlet end and the inlet end to obtain the sound transmission loss.

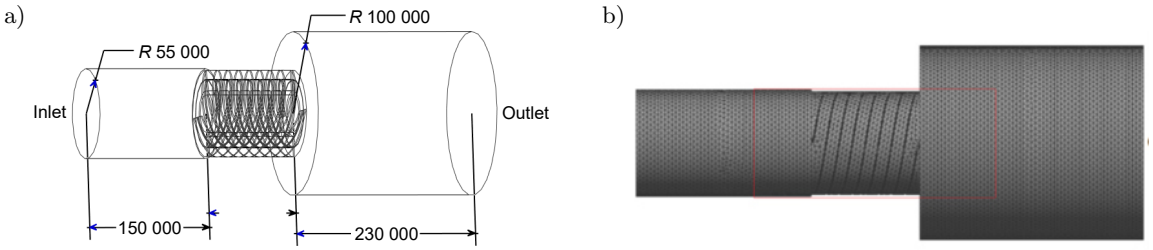

Fig. 7. Structure and grid of acoustic metamaterial muffling unit model: a) structure model, b) grid model.

Table 1. Model parameter.

Medium	Speed of sound	Inlet	Outlet	Wall type	Mesh type	Element size	Element count
Air	550 m/s	Acoustic excitation	Radiation boundary	Rigid	Tetrahedral	5 mm	164 000

3.2. Sound field analysis of noise reduction unit

Figure 8 shows the sound pressure level distribution of the single channel acoustic metamaterial unit and its vicinity at different frequencies. The phase difference between the plane wave at the entrance of the acoustic metamaterials and the acoustic wave vibration at the central through-hole after passing through the helical structure is generated. Since the length of the spiral channel is a fixed value, according to Eq. (3), different phase control results will be produced for waves of different frequencies. When there is a significant phase difference between the radiating wave at the exit of the central channel and the spiral channel, the result is shown in Fig. 8a. The destructive Fano interference generated by this strong coupling phenomenon significantly weakens the radiation of the sound wave in the far field, thus preventing the transmission of the sound wave. However, when there is no obvious phase difference or the phase difference is close to 2π, as shown in Fig. 8b, the sound waves of different acoustic channels can still produce the same direction upward vibration, resulting in the reduction of the noise reduction effect.

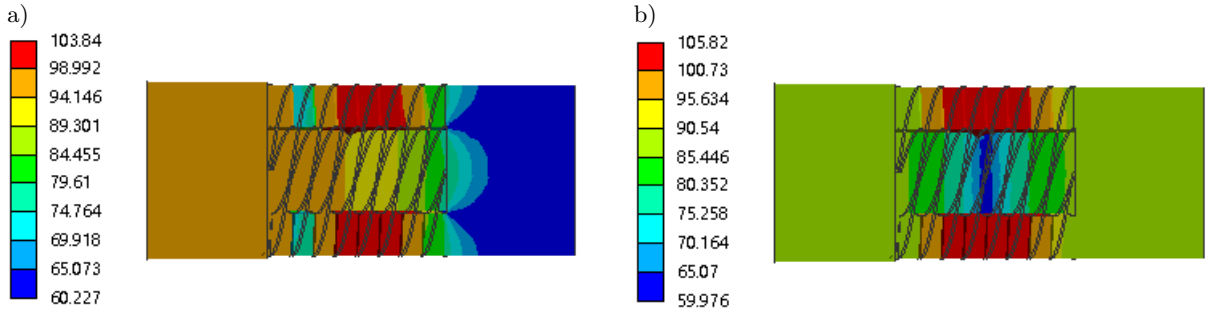

Fig. 8. Sound pressure level nephogram of single spiral channel at different frequencies: a) 760 Hz, b) 520 Hz.

For multi-channel structures, as shown in Fig. 9, different spiral radii have different acoustic refractive indices, resulting in different phase regulation results for plane incident waves at the same frequency, corresponding to different acoustic attenuation frequencies, which also makes the vibration environment more complex. Figure 9a shows the sound field distribution when there is a significant phase difference between the outer ring acoustic channel and the central channel, and when the coupled vibration is significantly different from the vibration of the inner ring acoustic channel. As shown in Fig. 9b, it is the sound field distribution when there is a significant phase difference between the inner ring acoustic channel and the central channel, and the coupled vibration is

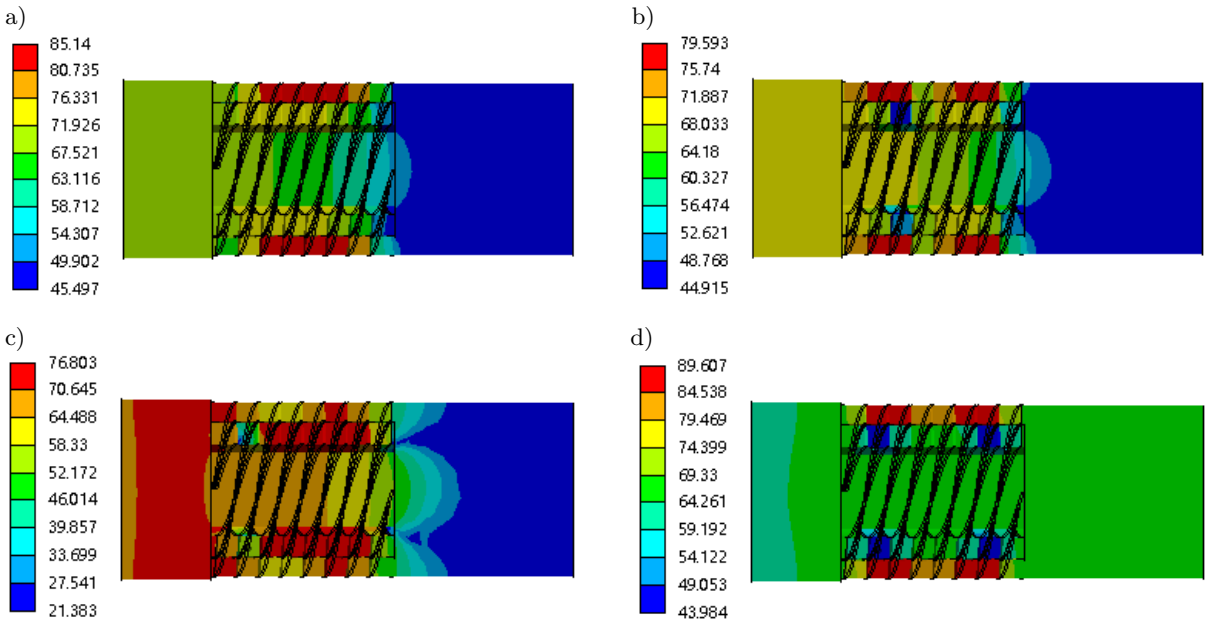

Fig. 9. Sound pressure level nephogram of double helix channel at different frequencies: a) 540 Hz, b) 920 Hz, c) 800 Hz, d) 1020 Hz.

significantly different from the vibration of the outer ring acoustic channel. In addition, there is also the influence of multi-channel coupled vibration, as shown in Fig. 9c, which refers to the sound field distribution when there is a significant phase difference between the inner ring and the outer ring acoustic channel, and when there is a significant phase difference between the coupled vibration and the central acoustic channel. Similarly, coupling vibration caused by small phase difference between the phase control result and the central channel may also occur, which greatly weakens the sound reduction effect, as shown in Fig. 9d, which refers to the resonance generated when the phase difference of each acoustic channel is a 2π multiple, reducing the difference in sound pressure between the outlet and the inlet and greatly reducing the sound reduction effect.

3.3. Transmission loss analysis of muffling unit

For three-channel acoustic metamaterials, the vibration becomes more complex, which greatly increases the difficulty of theoretical calculation and sound field analysis. Therefore, the acoustic simulation of transmission loss of different structure acoustic units is carried out to make a comparative analysis. As shown in Fig. 10a, for the case of a single track, due to the high central muffler frequency and the asymmetry of Fano interference, no obvious muffler below 740 Hz can be formed under the design structure size, which means that to achieve a lower frequency muffler, the length of the structure needs to be significantly increased. In order to match the impedance, it is also necessary to significantly increase the diameter of the structure, resulting in an increase in the size of the noise reduction structure. In the case of dual outer loop channels, as shown in Fig. 10b, although a narrowband passing frequency is increased compared with that of a single channel, the noise attenuation ability between 520 Hz and 730 Hz is significantly enhanced, thus obtaining a lower noise attenuation frequency. However, there are still some differences in the noise reduction intensity between 500 Hz to 740 Hz and 740 Hz to 1000 Hz. Through a large number of simulations, a three-channel sound attenuation structure can be obtained when the impedance of each channel is reasonably matched, and its transmission loss is shown in Fig. 10c. Although a narrowband passing frequency is added again, the transmission loss between 500 Hz and 1000 Hz is relatively uniform, and the width of each passing frequency is also reduced.

It can be seen that the three-channel noise reduction structural unit can obtain a lower noise reduction frequency on a wider noise reduction bandwidth, and then meet the noise reduction target requirements of 500 Hz to 1000 Hz. The dimensions of the acoustic metamaterial muffler were obtained as follows: inner diameter r_1 = 2.5 cm, outer diameter r = 5.5 cm, height l = 11.2 cm, spacer radii were 32 cm and 41 cm, respectively, and

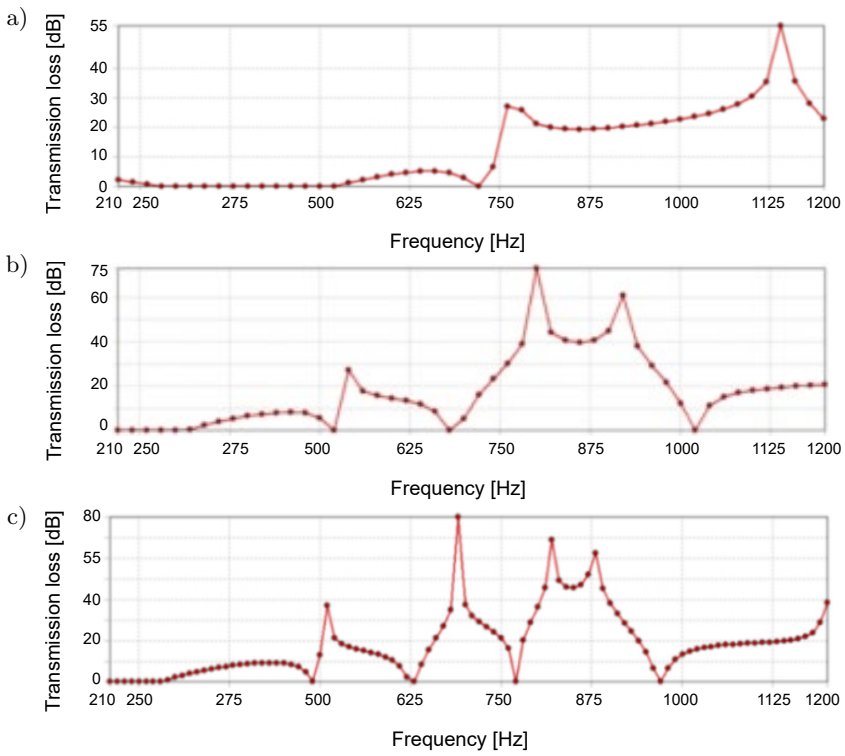

Fig. 10. Transmission loss of different spiral channel muffler chips at 210 Hz to 1200 Hz: a) single helix, b) double helix, c) triple helix.

spiral rotation angle was 3.6π. The structure has a transmission loss of more than 5 dB in the 93 % target noise attenuation frequency bandwidth, a transmission loss of more than 10 dB in the 85 % target noise attenuation frequency bandwidth, and a transmission loss of more than 20 dB in the 30 % target noise attenuation frequency bandwidth.

3.4. Multistage phase difference transfer loss analysis

The acoustic metamaterial noise reduction unit can also achieve multi-stage phase difference control at higher frequencies, so as to obtain the corresponding noise reduction ability, but this also makes the transmission loss curve more complicated. For this purpose, we conducted the test as shown in Fig. 11.

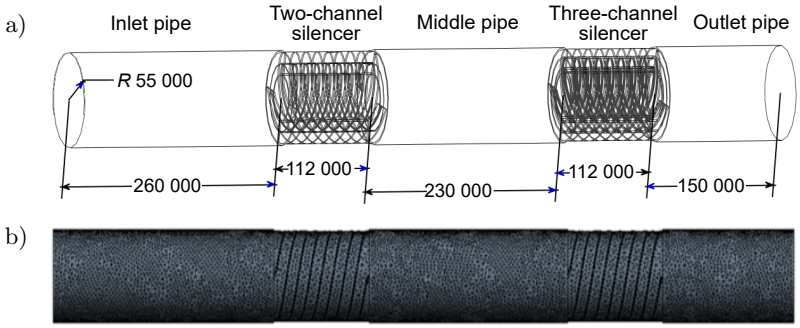

Fig. 11. Structure and grid of acoustic metamaterial muffling unit: a) structure model, b) grid model.

As shown in Fig. 12, when the phase difference of the sound field is $(2n+1)\pi$, the dipole vibration condition as shown in Eq. (11) can still be formed, which significantly increases the transmission loss of the acoustic metamaterial muffling unit, which means that the phase-regulated acoustic metamaterials can maintain effective muffling ability in a wider frequency range. It has obvious advantages over narrow band absorption with the fixed local resonance structure.

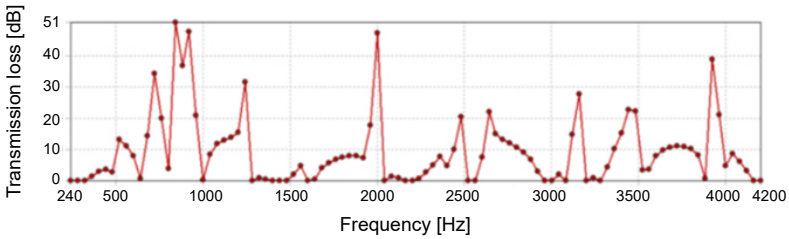

Fig. 12. Transmission loss at 240 Hz to 4200 Hz of three channel muffler chip.

3.5. Transmission loss analysis of combined structure of muffling unit

Through a number of different structures of the noise units in series form 1D linear combination, can also achieve a wider range of noise or in the rated target frequency band to obtain stronger noise reduction effect and more stable transmission loss. As shown in Fig. 13, when the three-channel muffling unit and the two-channel muffling unit are combined in series, due to the difference in the passing frequency of the two structural sounds, the three-channel muffling unit can be blocked by the two-channel muffling unit at the passing frequency and cannot radiate to the external field through a reasonable design. The vibration of the two-channel muffler through the frequency is greatly weakened at the entrance of the two-channel muffler due to the obstruction of the three-channel muffler, and it cannot radiate to the external field. Therefore, in the range of the target muffler frequency band, the passing frequency of the sound wave completely disappears, and a transmission loss of the full frequency band greater than 10 dB is obtained.

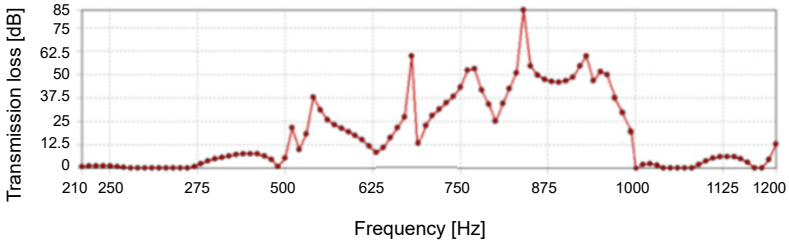

Fig. 13. Transmission loss of three channel and two channel muffling unit combination at 210 Hz to 1200 Hz.

4. Simulation analysis of flow field of muffling unit

4.1. Exhaust resistance analysis of muffling unit

According to the principle of internal combustion engine work, too high exhaust resistance on the one hand, will increase the piston pump gas work loss, on the other hand, will lead to cylinder exhaust pressure rise, residual exhaust gas increase, which will have an adverse effect on the fuel consumption rate and effective power of the internal combustion engine, therefore, the muffler must have good gas passage and small exhaust resistance.

In order to understand the fluid mechanics performance of the acoustic metamaterials muffling unit, a comparative analysis was conducted with the most common and simple-structured expanded muffling unit (expansion chamber size: radius 10 mm, length 20 mm) as a reference. As shown in Fig. 14a and Fig. 14b, the flow fields of the traditional expanded muffling unit and the acoustic metamaterial muffling unit are compared and analyzed through the fluent fluid dynamics analysis module in ANSYS Workbench 2020. The single-phase flow model is adopted. The expanded muffler uses a hexahedral unit grid with a grid size of 5 mm and a number of 55 000 grids, with a grid aspect ratio of 2.17. The acoustic muffling unit uses a tetrahedral to polyhedral unit grid with a grid size of 5 mm and a number of 40 400 grids, with a grid aspect ratio of 13.4. The grid models obtained are shown in Fig. 14c and Fig. 14d. The turbulence model adopts the standard $k-\varepsilon$ two-path model; when calculating, the inlet boundary condition is the velocity inlet, and the average inlet velocity is 70 m/s. The outlet boundary condition is a pressure outlet, and the wall boundary condition is an adiabatic non-slip wall. The key parameters for flow field simulation of muffling units is shown in Table 2.

a) Structure of the expanded muffling unit

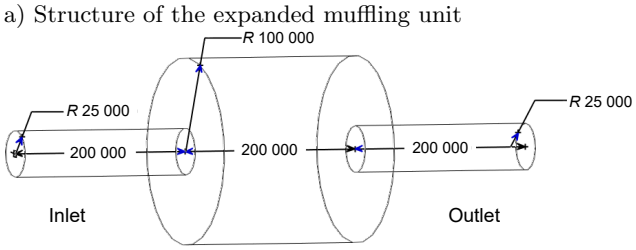

b) Structure of the acoustic metamaterial muffling unit

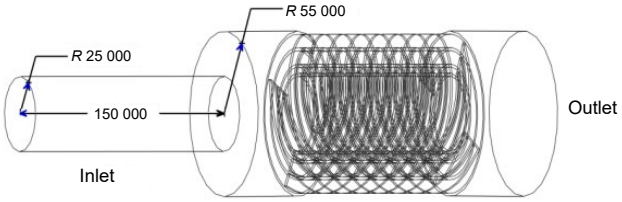

c) Grid of the expanded muffling unit

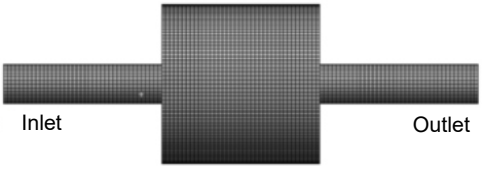

d) Grid of the acoustic metamaterial muffling unit

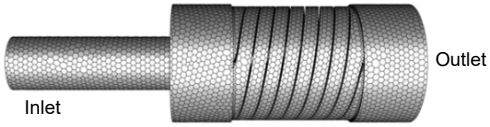

Fig. 14. Structure and grid of expanded muffling unit and acoustic metamaterial muffling unit.

Table 2. Key parameters for flow field simulation of muffling units.

Parameter type	Expanded muffling unit	Acoustic metamaterials muffling unit
Physical model	Single-phase flow model	Single-phase flow model
Mesh type	Hexahedral element mesh	Tetrahedral to polyhedral element mesh
Mesh size	5 mm	5 mm
Number of meshes	55 000	40 400
Mesh aspect ratio	2.17	13.4
Turbulence model	Standard $k-\varepsilon$ two-equation model	Standard $k-\varepsilon$ two-equation model
Inlet boundary condition	Velocity inlet, average velocity 70 m/s	Velocity inlet, average velocity 70 m/s
Outlet boundary condition	Pressure outlet	Pressure outlet
Wall boundary condition	Adiabatic non-slip wall	Adiabatic non-slip wall
Corresponding diagrams	Fig. 14a, Fig. 14c	Fig. 14b, Fig. 14d

As shown in Fig. 15, the cloud diagram of turbulent kinetic energy, when the inlet pipe diameter is the same, the energy loss of the expanding muffling unit mainly occurs at the outlet pipe of the cavity, which causes the change of the direction of the gas velocity vector at the outlet to a certain extent, causing resistance to gas flow. As the expansion length and diameter of the acoustic metamaterial muffler are obviously smaller than that of the expansion type muffler, the turbulence at the exit is not obvious, and the main turbulence is located at the end face of the outer ring. However, since the end face of the outer ring is a spiral ventilation structure, allowing a certain airflow to pass through, the turbulence intensity is significantly lower than that of the expansion type muffler. The energy dissipation of the acoustic metamaterial muffler is obviously lower than that of the expansion type muffler under the condition of pipeline gas flow, indicating that the structure is conducive to reducing the

a)

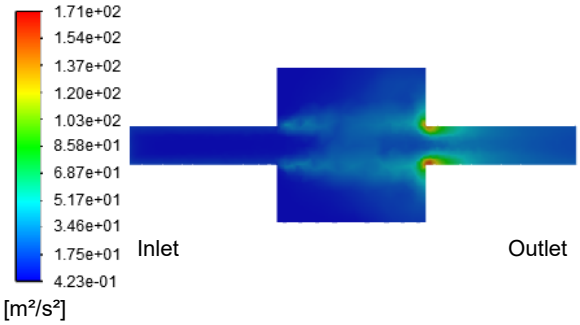

b)

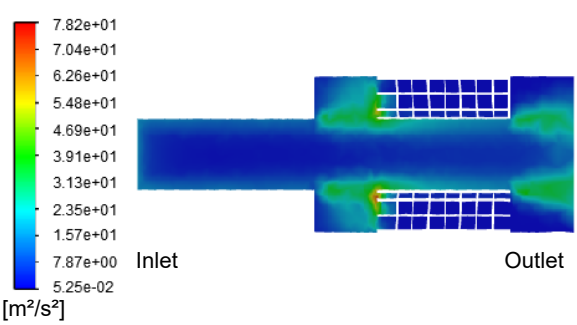

Fig. 15. Turbulent kinetic energy nephogram of different muffling units:
a) expanded muffling unit, b) acoustic metamaterial muffling unit.

transmission resistance. Meanwhile, the lower turbulent kinetic energy indicates that the acoustic metamaterial muffler is not easy to produce strong aerodynamic regeneration noise.

As can be seen from Fig. 16, after the gas in the inlet pipe of the expansion muffler enters the expansion chamber, the speed decreases significantly, which consumes a large amount of gas kinetic energy, resulting in a decrease in the dynamic pressure inside the pipeline. The pressure inside the chamber needs to be re-established to make the gas flow out quickly. This allows the kinetic energy of the gas in the pipeline to be preserved and maintains a high dynamic pressure of the gas, which is conducive to reducing the exhaust resistance.

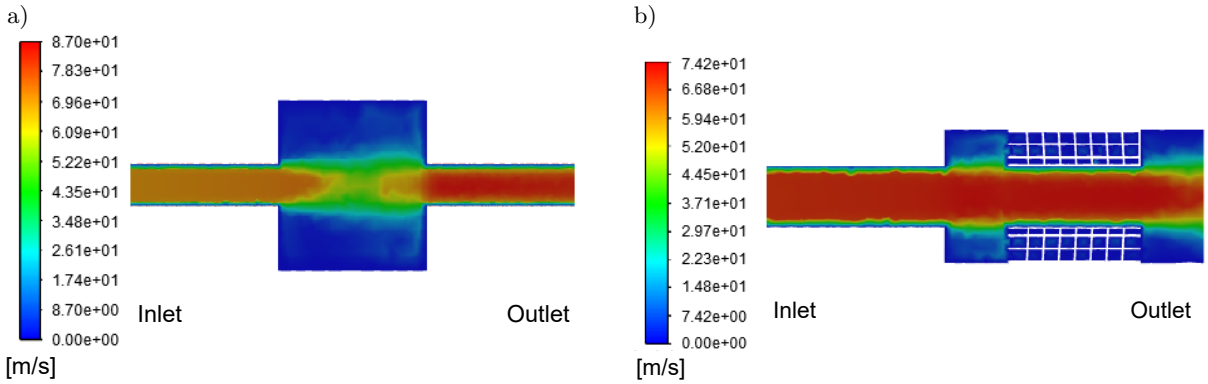

Fig. 16. Velocity nephogram of different muffling units: a) expanded muffling unit, b) acoustic metamaterial muffling unit.

By comparing the pressure loss of the two muffler devices, as shown in Fig. 17, under the condition of 70 m/s, the exhaust resistance of the expanded muffling unit can reach 2280 Pa, while the exhaust resistance of the acoustic metamaterials muffling unit is only 360 Pa. It can be seen that the volume of the acoustic metamaterials muffling unit is not only significantly smaller than that of the traditional muffling unit, but also that of the acoustic metamaterial muffling unit. Moreover, there are obvious advantages in exhaust resistance. It can be seen that while enhancing the noise reduction performance, the metamaterial muffler maintains the high kinetic energy characteristics of the gas in the central channel, avoiding the energy loss caused by the process of first dissipating and then establishing the gas kinetic energy in the expansion muffler, thereby suppressing the increase of equipment resistance and system back pressure. This is conducive to avoiding the increase in residual waste and the reduction of the charge coefficient caused by the poor exhaust of the engine due to the increased demand for noise reduction capacity, and can also reduce the pumping loss of the engine, ultimately achieving an improvement in the power and efficiency of the engine.

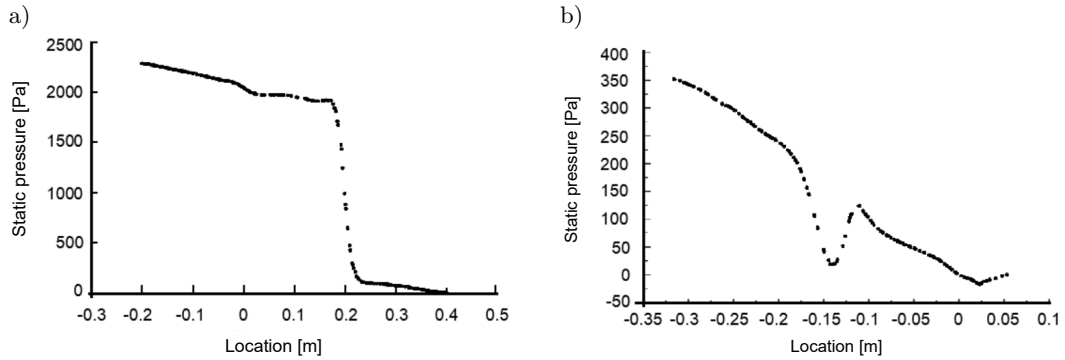

Fig. 17. Pressure loss on axis of different muffling units: a) acoustic metamaterial muffling unit, b) expanded muffling unit.

4.2. Analysis of exhaust resistance in series between traditional muffling unit and acoustic metamaterial muffling unit

For the muffler system, the best muffler effect often comes from the series muffler structure. Since the size parameters of the acoustic metamaterial muffling unit are more than the number of constraint formulas, the struc-

ture design has a multi-degree of freedom dimension relationship, which provides good conditions for the series with the traditional muffling unit. The series can be in the form of two muffler devices closely connected in series or the acoustic metamaterial muffling unit directly installed at the end of the pipeline, in which the exhaust resistance is the sum of the exhaust resistance of the two muffler structures directly installed at the end of the pipeline. Therefore, simulation is only carried out on the connected and series structure, as shown in Fig. 18. Two types of muffling units are connected in series without sacrificing too large volume of muffler. One end of the acoustic metamaterial muffler is connected to the inlet of the expansion muffler, the other end is connected to the air inlet, and the outlet of the expansion muffler is connected to the exhaust outlet to obtain the combined muffler structure.

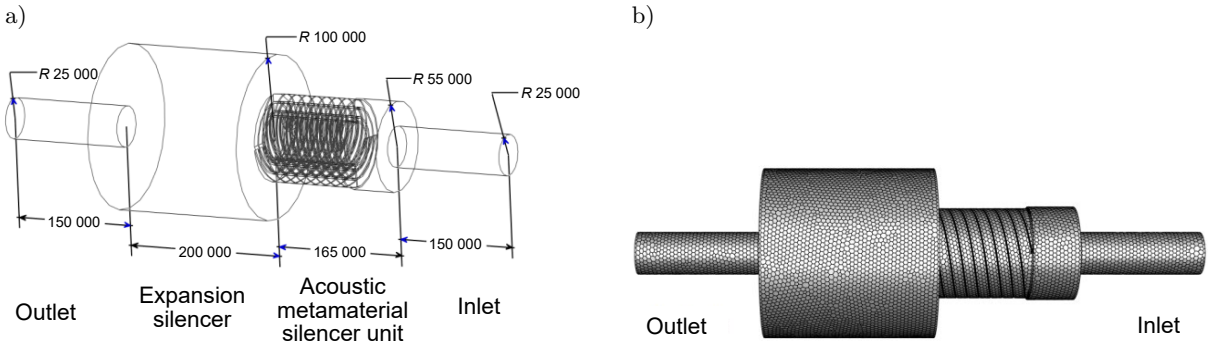

Fig. 18. Structure (a) and grid (b) of combined muffler models.

The velocity and turbulent kinetic energy cloud images are shown in Fig. 19 and Fig. 20. It can be seen that gas maintains a high flow speed in the pipe of the acoustic metamaterial muffler. At the same time, the side wall of the acoustic metamaterial muffler has a certain airflow passage, thus weakening the turbulence of gas entering the expansion type and reducing energy dissipation, so that the flow speed of gas in the axis of the expansion chamber is slightly higher than that of the independent expansion muffler structure. To a certain extent, this is conducive to maintaining the kinetic energy of the gas and reducing the exhaust loss, but as a result, the gas obtains a higher speed at the exit, and also forms a stronger turbulence, resulting in a certain energy dissipation.

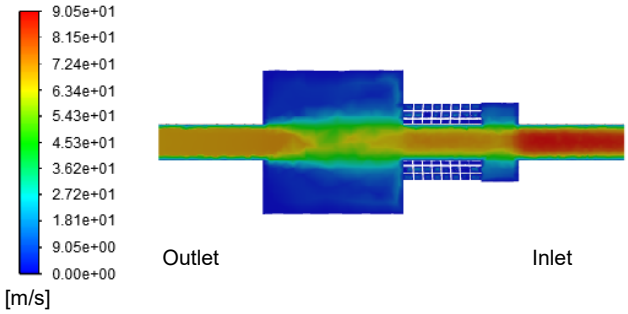

Fig. 19. Velocity nephogram of combined muffler.

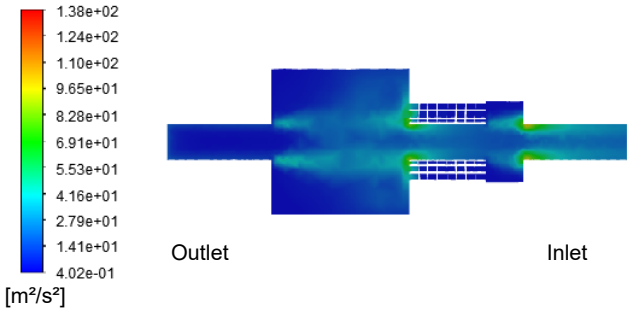

Fig. 20. Cloud diagram of turbulent kinetic energy of combined muffler.

As shown in Fig. 21, the overall curve is consistent with but slightly higher than that of the expansion muffler. At 70 m/s, the exhaust loss is 2650 Pa. Compared with the 2280 Pa exhaust loss of the expansion muffler structure alone, the exhaust resistance of the acoustic metamaterial muffling unit only increases 370 Pa, indicating that in the series structure, the exhaust resistance of the acoustic metamaterial muffling unit only increases 370 Pa. Compared with when used alone, in the case of combined use, the resistance increase caused by the acoustic metamaterial muffler remains linearly rising. Under combined use conditions, there will be no mutual interference of resistance, and only a very small resistance cost is needed to significantly improve the noise reduction performance of the muffler.

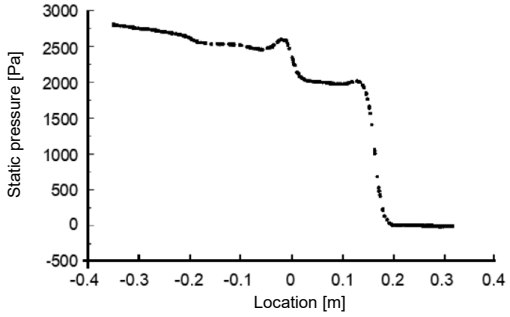

Fig. 21. Pressure loss on the axis of combined muffler.

5. Noise reduction performance test

5.1. Experimental conditions and methods

In order to test the acoustic performance of the acoustic metamaterial muffler, a single cylinder diesel engine model ZS1105 was used as a prototype to compare the noise difference before and after the original muffler was added to the acoustic metamaterial muffler.

Main equipment required for the experiment: one internal combustion engine testing machine, one muffler straight tube, one original muffler, one ceramic 3D printed three-channel acoustic metamaterial muffling unit, as shown in Fig. 22a, and one AWA6228+ multifunctional sound level meter of Qingdao Juchuang. The acoustic metamaterial muffler and the original muffler can be combined in various ways. In this experiment, the acoustic metamaterial muffler is installed directly at the end of the original muffler, as shown in Fig. 22b.

a) b)

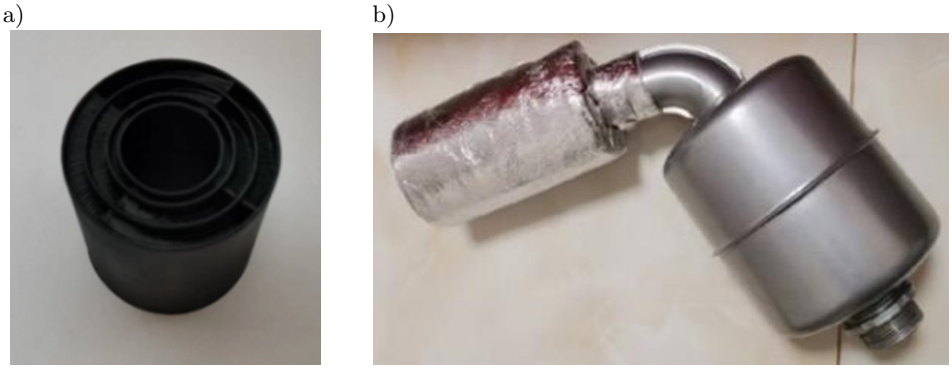

Fig. 22. Acoustic metamaterial muffling unit (a) and its combined structure with original muffler (b).

5.2. Lab process

The noise suppression performance test is carried out according to '7.2 Laboratory Measurement Method' in GB/T 4759-2009 'Internal Combustion Engine exhaust muffler – Measurement Method.' First, in order to reduce the impact of other types of diesel engine noise on the test results, a retaining wall is set up, the diesel engine and

the muffler are placed on both sides of the retaining wall, and then a hole is drilled in the retaining wall and the diesel engine and the muffler are connected through a straight pipe. After the diesel engine ran stably for 15 min, the diesel engine speed was set to 2200 r/min, and the exhaust noise signal was recorded with a sound level meter at 45° at the exhaust pipe outlet and 0.5 m away from the exhaust pipe outlet. The sampling frequency was 1/3 in the frequency range of 31.5 Hz to 4000 Hz, and two experiments were carried out. The measured results were averaged. The acoustic metamaterial muffling units installed in series with the straight pipe without muffler, the original muffler, and the original muffler were respectively tested for noise, as shown in Fig. 23.

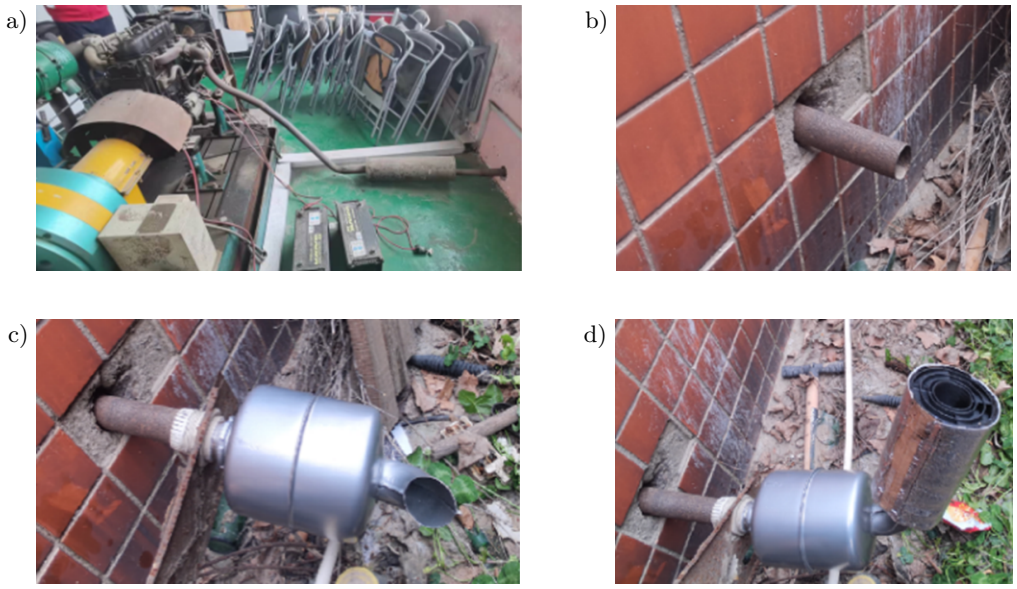

Fig. 23. Experimental test conditions: a) indoor testing machine, b) exhaust straight pipe, c) expanding muffler, d) combined muffler.

5.3. Performance test results

The noise test results are obtained, as shown in Fig. 24, when the speed is 2200 r/m, the 1/3 octave sound pressure level in the range of 25 Hz to 4000 Hz. The noise pressure level at different frequencies shows that the noise reduction effect of the original muffler starts to increase significantly after 1000 Hz, and before 1000 Hz, the transmission loss is obviously low, while after the series Acoustic metamaterial noise reduction unit, the noise reduction effect is not obvious below the frequency of 250 Hz. Between 250 Hz and 500 Hz, the transmission loss

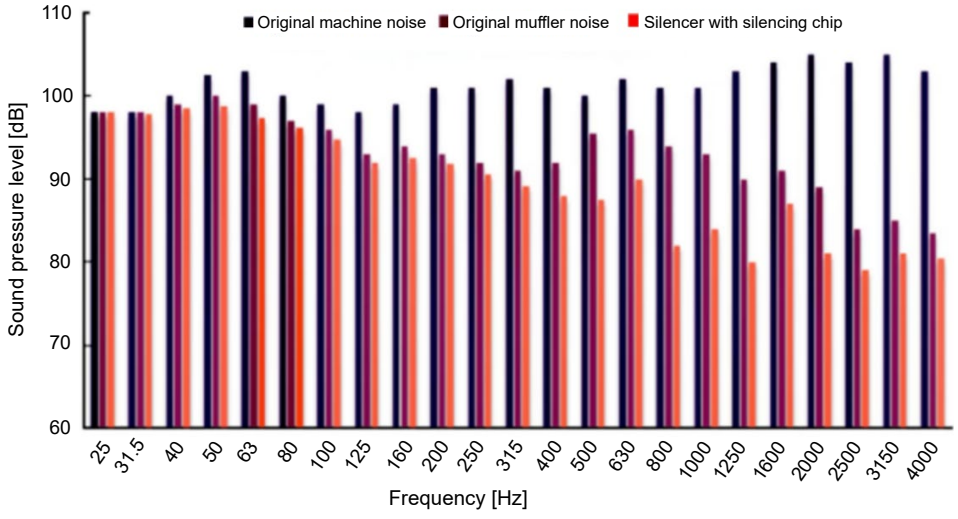

Fig. 24. 1/3 octave sound pressure level under different muffler conditions.

gradually increases, which is caused by the interference of sound waves to a certain extent caused by dipole vibration generated by different acoustic channels. At this stage, although the phase difference between the vibration phase of each channel and that of the central airflow channel is less than $\pi/2$, it gradually expands, showing that the transmission loss gradually increases and the noise reduction ability gradually increases. After 500 Hz, interference conditions are formed, and the transmission loss begins to increase significantly. In the target noise reduction frequency band, the insertion loss of 5 dB to 15 dB is formed. After 1000 Hz, the transmission loss gradually decreases as the phase difference becomes larger. It shows that the multipole vibration caused by the second and above phase difference of sound wave occurs in this frequency stage.

The final noise is compared with the loudness curve of NR90, as shown in Fig. 25. After the addition of the acoustic metamaterial muffling unit, the overall exhaust noise level is significantly lower than that of the N90 curve after the excessive noise at the stage of 500 Hz to 1000 Hz is eliminated, and the noise reduction of the frequency band with insufficient noise reduction under the original muffler condition is realized. Noise reduction that significantly exceeds the loudness curve can significantly reduce the loudness of noise emissions.

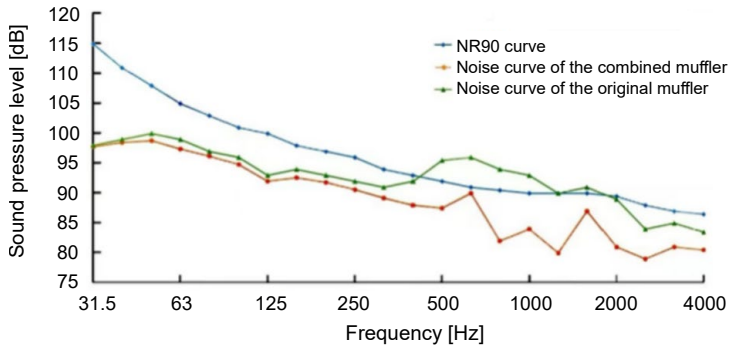

Fig. 25. Comparison between NR90 curve and noise curve after muffling.

It can be seen that the acoustic metamaterials can achieve noise reduction in the frequency band of 500 Hz to 1000 Hz, and the frequency band above 1000 Hz can achieve certain noise reduction ability through the interference of multi-order frequencies. Its advantage is that through structural adjustment and design, higher noise reduction ability can be obtained in the frequency where noise reduction is difficult. When the muffler is used alone, there will be obvious difference in transmission loss at different frequencies, but when combined with other muffler structures, it can carry out targeted muffler without significantly increasing the exhaust resistance, so as to solve the problem of insufficient muffler at some frequencies.

6. Conclusion

In this paper, according to the structural characteristics of internal combustion engine exhaust pipe and the performance requirements of exhaust noise reduction, the acoustic model is established by using the equivalent medium theory, and the phase control of sound field is realized by means of space winding, and the design of multi-channel helical metamaterials noise reduction unit is completed. The mechanism and performance of noise reduction are studied through acoustic simulation and experimental tests, and the following conclusions are drawn:

1. The acoustic metamaterial muffler adopts a spiral coil structure, which has a high space utilization rate, and adopts a multi-spiral channel structure, which reduces the asymmetric influence of Fano interference, and obtains obvious low and medium frequency muffler ability in the compact structure size.
2. The acoustic metamaterial unit realizes the change of acoustic refractive index in the equivalent acoustic region by means of phase regulation, and obtains the multi-pole vibration interference condition at the exit of the acoustic structure, which not only has obvious noise reduction effect at the target noise reduction frequency, but also can obtain obvious noise reduction ability at the high-order phase difference frequency. A stronger ability to eliminate sound without significant frequency can be obtained.

3. The acoustic metamaterial unit has a low exhaust resistance. Under the condition of single use or series use, the exhaust resistance is only 360 Pa to 370 Pa when the exhaust speed is 70 m/s, which has obvious advantages over the traditional noise reduction structure.

In summary, the multi-helical channel phase control acoustic metamaterial muffler has a good performance in terms of structure size, muffler performance, muffler frequency and exhaust resistance, and the structural design is flexible, so it will have a good application prospect in exhaust noise reduction.

Fundings

This work was supported by the National Natural Science Foundation of China (52475354) and the Industry-University Collaborative Education Project of the Ministry of Education (221001414112514).

Conflict of interests

The authors declare that they have no known competing financial interests or personal relationships that could have appeared to influence the work reported in this paper.

Authors' contributions

All authors contributed equally to this work, reviewed, and approved the final manuscript.

References

1. Araujo E.S., Pestana R.C. (2024), A numerical scheme based on the Taylor expansion and Lie product formula for the second-order acoustic wave equation and its application in seismic migration, *Geophysical Prospecting*, **72**(5): 1745–1763, https://doi.org/10.1111/1365-2478.13481.
2. Bai C., Wu F., Wang J., Jiang J. (2023), A broadband low-frequency muffler based on neural network method and Helmholtz resonator with helical neck, *Journal of Vibration and Control*, **29**(17–18): 3942–3951, https://doi.org/10.1177/10775463221107197.
3. Chen N. *et al.* (2024), Research on prediction of yellow flesh peach firmness using a novel acoustic real-time detection device and Vis/NIR technology, *LWT*, **209**: 116772, https://doi.org/10.1016/J.LWT.2024.116772.
4. Chen Z., Ji Z., Huang H. (2020), Acoustic impedance of perforated plates in the presence of fully developed grazing flow, *Journal of Sound and Vibration*, **485**: 115547, https://doi.org/10.1016/j.jsv.2020.115547.
5. Dalla Nora M., Lanzanova T.D.M., Zhao H. (2016), Effects of valve timing, valve lift and exhaust backpressure on performance and gas exchanging of a two-stroke GDI engine with overhead valves, *Energy Conversion and Management*, **123**: 71–83, https://doi.org/10.1016/j.enconman.2016.05.059.
6. Fang N. *et al.* (2006), Ultrasonic metamaterials with negative modulus, *Nature Materials*, **5**(6): 452–456, https://doi.org/10.1038/nmat1644.
7. Ghaffarivardavagh R., Nikolajczyk J., Anderson S., Zhang X. (2019), Ultra-open acoustic metamaterial muffler based on Fano-like interference, *Physical Review B*, **99**(2): 024302, https://doi.org/10.1103/PhysRevB.99.024302.
8. Guo J., Fang Y., Qu R., Zhang X. (2023), Development and progress in acoustic phase-gradient metamaterials for wavefront modulation, *Materials Today*, **66**: 321–338, https://doi.org/10.1016/j.mattod.2023.04.004.
9. Jiang T., Han Q., Li C. (2023), Topologically tunable local-resonant origami metamaterials for wave transmission and impact mitigation, *Journal of Sound and Vibration*, **548**: 117548, https://doi.org/10.1016/j.jsv.2022.117548.
10. Kheybari M., Ebrahimi-Nejad S. (2019), Locally resonant stop band acoustic metamaterial muffler with tuned resonance frequency range, *Materials Research Express*, **6**(2): 025802, https://doi.org/10.1088/2053-1591/aaed4b.
11. Khodabakhsh S., Movahhedy M.R., Mohammadi K. (2025), A Helmholtz resonator based on spiral neck acoustic metamaterial for noise reduction, *Applied Acoustics*, **240**: 110957, https://doi.org/10.1016/j.apacoust.2025.110957.
12. Kumar S., Lee H.P. (2020), Recent advances in acoustic metamaterials for simultaneous sound attenuation and air ventilation performances, *Crystals*, **10**(8): 686, https://doi.org/10.3390/cryst10080686.

13. Lee J.K., Oh K.S., Lee J.W. (2020), Methods for evaluating in-duct noise attenuation performance in a muffler design problem, *Journal of Sound and Vibration*, **464**: 114982, https://doi.org/10.1016/j.jsv.2019.114982.

14. Li L., Diao Y., Wu H., Jiang W. (2022), Thickness-designable acoustic metamaterial for passive phased arrays, *Applied Acoustics*, **198**: 108942, https://doi.org/10.1016/j.apacoust.2022.108942.

15. Li P., Yao S., Zhou X., Huang G., Hu G. (2014), Effective medium theory of thin-plate acoustic metamaterials, *The Journal of the Acoustical Society of America*, **135**(4): 1844–1852, https://doi.org/10.1121/1.4868400.

16. Li S., Lan Y., Hong L. (2024), A method to analyze the radiation characteristics of a liquid column resonance transducer based on fluid motion, *The Journal of the Acoustical Society of America*, **155**(1): 252–261, https://doi.org/10.1121/10.0024339.

17. Liao D., Cao H., Li S., Cheng W., Yan X., An C. (2024), Study on the control of flow field by resonance acoustic mixing technology for purification of high performance spherical HATO crystals, *Separation and Purification Technology*, **339**: 126688, https://doi.org/10.1016/j.seppur.2024.126688.

18. Lin D.K. *et al.* (2024), An acoustic impedance design method for tubular structures with broadband sound insulations and efficient air ventilation, *Applied Acoustics*, **220**: 109983, https://doi.org/10.1016/j.apacoust.2024.109983.

19. Liu M., Li P., Du Q., Peng P. (2019), Reflected wavefront manipulation by acoustic metasurfaces with anisotropic local resonant units, *EPL*, **125**(5): 54004, https://doi.org/10.1209/0295-5075/125/54004.

20. Liu Y. *et al.* (2020), Three-dimensional fractal structure with double negative and density-near-zero properties on a subwavelength scale, *Materials & Design*, **188**: 108470, https://doi.org/10.1016/j.matdes.2020.108470.

21. Lu T., Li Z., Zhang Y. (2025), Broadband low-transmission study of ventilation metasurfaces based on Archimedean spirals, *Applied Acoustics*, **228**: 110335, https://doi.org/10.1016/j.apacoust.2024.110335.

22. Martos F.J., Soriano J.A., Braic A., Fernández-Yáñez P., Armas O. (2023), A CFD modelling approach for the operation analysis of an exhaust backpressure valve used in a Euro 6 Diesel engine, *Energies*, **16**(10): 4112, https://doi.org/10.3390/en16104112.

23. Mohamad B., Karoly J., Zelentsov A., Amroune S. (2021), Investigation of perforated tube configuration effect on the performance of exhaust mufflers with mean flow based on three-dimensional analysis, *Archives of Acoustics*, **46**(3): 561–566, https://doi.org/10.24425/aoa.2021.138148.

24. Naify C.J., Chang C.M., McKnight G., Nutt S.R. (2012), Scaling of membrane-type locally resonant acoustic metamaterial arrays, *The Journal of the Acoustical Society of America*, **132**(4): 2784–2792, https://doi.org/10.1121/1.4744941.

25. Narayan S., Kaisan U.M., Abubakar S. (2021), A review of vibro-acoustic techniques for control of combustion engine noise, *Journal of Applied Engineering Science*, **19**(4): 880–885, https://doi.org/10.5937/JAES0-29675.

26. Orazbayev B., Fleuly R. (2020), Far-field subwavelength acoustic imaging by deep learning, *Physical Review X*, **10**(3): 031029, https://doi.org/10.1103/PhysRevX.10.031029.

27. Shaikh S. *et al.* (2024), Acoustic propagation and transmission loss analysis in shallow water of Northern Arabian Sea, *Journal of Marine Science and Engineering*, **12**(12): 2256, https://doi.org/10.3390/jmse12122256.

28. Su H., Wu P., Xue J., Zhang Y., Zhang H. (2020), Analysis of flow field characteristics and structure optimization of the split-stream rushing muffler for diesel engine, *Noise Control Engineering Journal*, **68**(1): 101–111, https://doi.org/10.3397/1/37688.

29. Sun M., Fang X., Mao D., Wang X., Li Y. (2020), Broadband acoustic ventilation barriers, *Physical Review Applied*, **13**(4): 044028, https://doi.org/10.1103/PhysRevApplied.13.044028.

30. Wan C. *et al.* (2023), A low-complexity multi-channel active noise control system using local secondary path estimation and clustered control strategy for vehicle interior engine noise, *Mechanical Systems and Signal Processing*, **204**: 110786, https://doi.org/10.1016/j.ymssp.2023.110786.

31. Wang C., Lu Z., Zhang K. (2012), Small-hole arrays of ceramic material manufactured by micro powder injection molding, *The International Journal of Advanced Manufacturing Technology*, **59**(9–12): 969–976, https://doi.org/10.1007/s00170-011-3570-5.

32. Wang C., Zhao H., Wang Y., Zhong J., Yu D., Wen J. (2024), Topology optimization of chiral metamaterials with application to underwater sound insulation, *Applied Mathematics and Mechanics*, **45**(7): 1119–1138, https://doi.org/10.1007/s10483-024-3162-8.

33. Xiao D.W., Cheng J.F., Zhang J.Z. (2013), Blind DOA estimation based on single acoustic vector hydrophone, *Advanced Materials Research*, **2428**(706–708): 678–681, https://doi.org/10.4028/www.scientific.net/AMR.706-708.678.

34. Xu C., Guo H., Chen Y., Dong X., Ye H., Wang Y. (2021), Study on broadband low-frequency sound insulation of multi-channel resonator acoustic metamaterials, *AIP Advances*, **11**(4): 045321, https://doi.org/10.1063/5.0047416.

35. Xu Z., Fang Y., Wang Z. (2025), Enhanced fano-type broadband acoustic ventilated muffler with arbitrary geometrical configurations, *Frontiers in Physics*, **13**: 1586858, https://doi.org/10.3389/fphy.2025.1586858.

36. Yang M., Ma G., Yang Z., Sheng P. (2013), Coupled membranes with doubly negative mass density and bulk modulus, *Physical Review Letters*, **110**(13): 134301, https://doi.org/10.1103/PhysRevLett.110.134301.

37. Yang M., Ma G., Wu Y., Yang Z., Sheng P. (2014), Homogenization scheme for acoustic metamaterials, *Physical Review B*, **89**(6): 064309, https://doi.org/10.1103/PhysRevB.89.064309.

38. Ye Y.-R., Wang X.-P., Chen T.-N., Chen Y.-Y. (2020), Step-by-step structural design methods for adjustable low-frequency sound insulation based on infinite plate-type acoustic metamaterial panel, *Modern Physics Letters B*, **34**(21): 6–18, https://doi.org/10.1142/S0217984920502206.

39. Zeng H.-C., Luo C.-R., Chen H.-J., Zhai S.-L., Ding C.-L., Zhao X.-P. (2013), Flute-model acoustic metamaterials with simultaneously negative bulk modulus and mass density, *Solid State Communications*, **173**: 14–18, https://doi.org/10.1016/j.ssc.2013.08.017.

40. Zhang Y., Wu P., Ma Y., Su H., Xue J. (2018), Analysis on acoustic performance and flow field in the split-stream rushing muffler unit, *Journal of Sound & Vibration*, **430**: 185–195, https://doi.org/10.1016/j.jsv.2018.04.025.

41. Zhang X., Zhao C., Wang P., Chen R. (2024), Combined acoustic metamaterial design based on multi-channel Fano resonance effect, *Journal of Applied Physics*, **136**(1): 013105, https://doi.org/10.1063/5.0211050.